AD-A112 012 AEROSPACE CORP EL SEGUNDO CA LAB OPERATIONS F/G 9/1
BARIUM TRANSPORT PROCESS IN IMPREGNATED DISPENSER CATHODES.(U)
JAN 82 A A FOTE, K T LUEY F04701-81-C-0082
UNCLASSIFIED TR-0082(2945-02)-1 SD-TR-81-102 NL

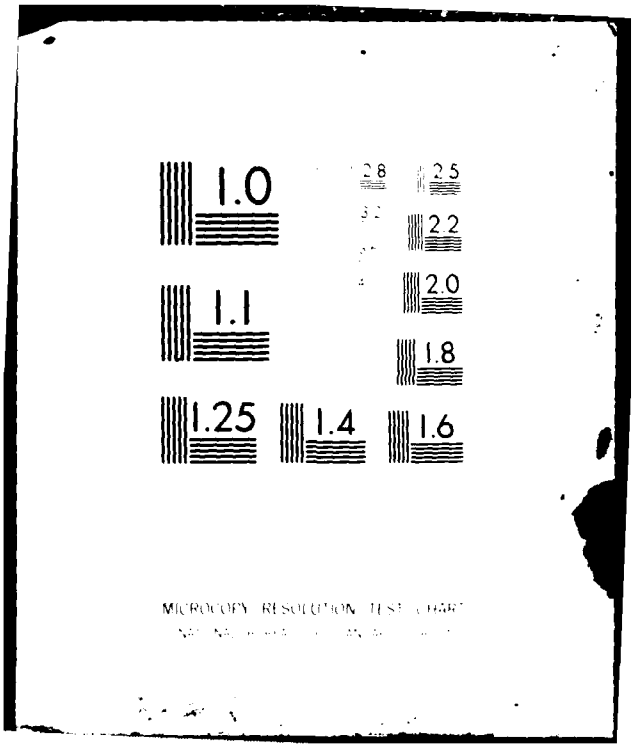
1.0
1.1
1.25
1.4
1.6
2.8
2.5
2.2
2.0
1.8
MICROCOPY RESOLUTION TEST CHART

(5)

REPORT SD-TR-81-102

AD A112012

Barium Transport Process in Impregnated Dispenser Cathodes

Prepared by
A. A. FOTE and K. T. LUEY
Laboratory Operations
The Aerospace Corporation
El Segundo, Calif. 90245

25 January 1982

APPROVED FOR PUBLIC RELEASE;
DISTRIBUTION UNLIMITED

Prepared for

SPACE DIVISION
AIR FORCE SYSTEMS COMMAND
Los Angeles Air Force Station
P.O. Box 92960, Worldway Postal Center
Los Angeles, Calif. 90009

This interim report was submitted by The Aerospace Corporation, El Segundo, CA 90245, under Contract No. F04701-81-C-0082 with the Space Division, Deputy for Technology, P.O. Box 92960, Worldway Postal Center, Los Angeles, CA 90009. It was reviewed and approved for The Aerospace Corporation by S. Feuerstein, Director, Chemistry and Physics Laboratory. Capt David Dise, SD/YLXT, was the Project Officer for the Mission-Oriented Investigation and Experimentation (MOIE) Program.

This report has been reviewed by the Public Affairs Office (PAS) and is releasable to the National Technical Information Service (NTIS). At NTIS, it will be available to the general public, including foreign nations.

This technical report has been reviewed and is approved for publication. Publication of this report does not constitute Air Force approval of the report's findings or conclusions. It is published only for the exchange and stimulation of ideas.

David Dise

David Dise, Captain, USAF
Project Officer

Florian P. Meinhardt

Florian P. Meinhardt, Lt Col, USAF
Director of Advanced Space Development

FOR THE COMMANDER

Norman W. Lee

Norman W. Lee, Jr., Colonel, USAF
Deputy for Technology

UNCLASSIFIED

SECURITY CLASSIFICATION OF THIS PAGE (When Data Entered)

REPORT DOCUMENTATION PAGE		READ INSTRUCTIONS BEFORE COMPLETING FORM
1. REPORT NUMBER SD-TR-81-102	2. GOVT ACCESSION NO. AD-A112 012	3. RECIPIENT'S CATALOG NUMBER
4. TITLE (and Subtitle) BARIUM TRANSPORT PROCESSES IN IMPREGNATED DISPENSER CATHODES		5. TYPE OF REPORT & PERIOD COVERED 6. PERFORMING ORG. REPORT NUMBER TR-0082(2945-02)-1
7. AUTHOR(s) Alfred A. Fote and Kenneth T. Luey		8. CONTRACT OR GRANT NUMBER(s) F04701-81-C-0082
9. PERFORMING ORGANIZATION NAME AND ADDRESS The Aerospace Corporation El Segundo, Calif. 90245		10. PROGRAM ELEMENT, PROJECT, TASK AREA & WORK UNIT NUMBERS
11. CONTROLLING OFFICE NAME AND ADDRESS Space Division Air Force Systems Command Los Angeles, Calif. 90009		12. REPORT DATE 25 January 1982 13. NUMBER OF PAGES 22
14. MONITORING AGENCY NAME & ADDRESS(if different from Controlling Office)		15. SECURITY CLASS. (of this report) Unclassified 15a. DECLASSIFICATION/DOWNGRADING SCHEDULE

16. DISTRIBUTION STATEMENT (of this Report)

Approved for public release; distribution unlimited.

17. DISTRIBUTION STATEMENT (of the abstract entered in Block 20, if different from Report)

18. SUPPLEMENTARY NOTES

19. KEY WORDS (Continue on reverse side if necessary and identify by block number)

Dispenser
Surface
Barium
Cathodes
Diffusion

20. ABSTRACT (Continue on reverse side if necessary and identify by block number)

An impregnated dispenser cathode is a dynamic system in which the continuous loss of barium from the emitting surface must be compensated for by a surface diffusion supply process. A review of the effect of these processes on certain surface characteristics is given in this paper. A derivation is then presented indicating that inside the porous matrix, surface diffusion may be the dominant transport mode rather, than the Knudsen flow, which has been emphasized previously. - -

DD FORM 1473 (FACSIMILE)

UNCLASSIFIED

SECURITY CLASSIFICATION OF THIS PAGE (When Data Entered)

19. KEY WORDS (Continued)

20. ABSTRACT (Continued)

We discuss our experimental approach for determining the surface diffusion coefficient and present data that indicate that the surface diffusion transport process can be severely slowed by some surface species, which most likely is oxygen.

CONTENTS

FIGURES

I. INTRODUCTION

High electron emission currents from tungsten dispenser cathodes are achieved when a film of barium and oxygen is present on the emitting surface [1-3]. To maintain this film at operating temperatures, the continuous loss of barium resulting from evaporation must be compensated for by the transport of fresh barium from the porous tungsten matrix in which it has been impregnated [4]. Surface diffusion and evaporation are important, both in the spreading of the barium over the emitting surface and in the flow inside the pores. Our studies have been directed toward the development of a detailed model of the mechanics of these processes and the clarification of their effects on dispenser cathode operation and design criteria.

II. THEORETICAL CONSIDERATIONS

A. TRANSPORT OVER THE EMITTING SURFACE

An idealized version of a pore that opens onto the emitting cathode surface is shown in Figure 1. The barium distribution on the surface itself is described by the differential equation

$$\frac{d\theta}{dt} = \vec{\nabla} \cdot D \vec{\nabla} \theta - \theta^{\gamma}/\tau, \quad \theta < 1 \tag{1}$$

where

θ = coverage with $\theta = 1$ corresponding to one monolayer

D = coefficient of surface diffusion

τ = mean residence time before a barium atom desorbs from the surface when $\theta = 1$

γ ≈ an empirical factor ≃ 4.5 [5]

This equation states that the time evolution of the coverage is governed by a diffusion-controlled supply and an evaporation-controlled loss, with the expression for the latter as proposed by Langmuir and verified by many others [5]. We confine θ to values less than or equal to 1, because most of the investigators have reported submonolayer-to-monolayer coverage of barium on the emitting surface of impregnated cathodes [1,6].

Under quasi-equilibrium conditions, $d\theta/dt = 0$, the coverage is determined by the equation

$$\vec{\nabla} \cdot D \vec{\nabla} \theta = \frac{\theta^{\gamma}}{\tau} \tag{2}$$

For a surface with a random array of pore openings, this equation must be solved numerically. However, we can obtain some understanding of the expected behavior of θ if we treat the simpler case of an isolated, one-dimensional pore and take D as independent of θ. Thus, Eq. (2) becomes

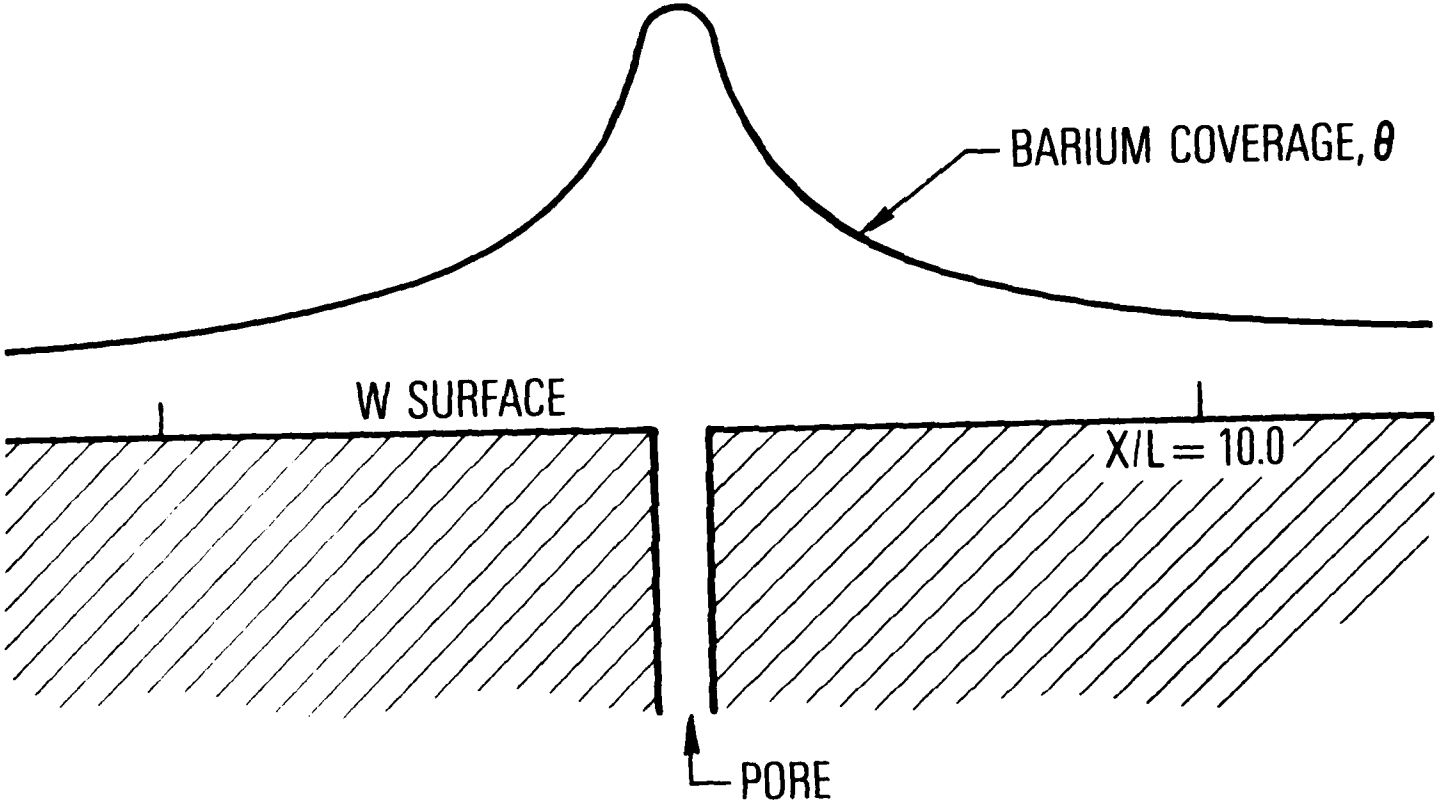

Fig. 1. Idealized Version of a Pore Opening Onto a Dispenser Cathode Surface. The barium coverage, as plotted, is from Eq. (4)

$$D \frac{d^2\theta}{dx^2} = \frac{\theta^\gamma}{\tau} \tag{3}$$

If we impose the boundary condition that $\theta = 1$ at $x = 0$ (at the lip of the pore), we obtain the solution

$$\theta = \left[1 + \frac{(\gamma - 1)}{\sqrt{2}\,(\gamma + 1)} \frac{x}{L}\right]^{-\frac{2}{\gamma-1}} \tag{4}$$

where we have introduced the critical length parameter L by

$$L = \sqrt{D\tau} \tag{5}$$

Equation (4) is plotted in Figure 1. As defined, the parameter L is the average distance a barium atom will travel along the surface before it desorbs when $\theta = 1$.

From Eq. (4) it is evident that θ is dependent only on the ratio x/L. Thus, the distribution profile scales in the x direction with L. This scaling behavior is also found in the more realistic situation of two dimensions with D dependent on θ. In this case, if we write $D(\theta) = Df(\theta)$, $f(1) = 1$, it is easy to show that in the two-dimensional differential equation, Eq. (2), the distance parameter scales with $L = \sqrt{D\tau}$. From this observation, we make our first conclusion: the average coverage on a cathode surface that contains an array of pores is a function of the ratio $\sqrt{D\tau}/d$, where d is the average spacing between the pores.

In addition to the average coverage, a parameter of interest for cathode operation is the recovery time τ_R. This is the time required for a cathode to recover from a transient loss of barium. For a system of pores that are spaced close enough so that $\sqrt{D\tau} > d$, yielding $\theta \approx 1$ everywhere, the recovery time is proportional to the time required for a barium atom to cover the distance d/2. Thus, under these conditions, we expect to have

$$\tau_R \approx \frac{(d/2)^2}{D} \tag{6}$$

The supply rate required to maintain the equilibrium condition described by Eq. (4) is given by

$$J \text{ (atoms/sec)} = -\alpha D \left.\frac{d\theta}{dx}\right|_{x = 0} \tag{7}$$

where α is the number of atoms per unit surface area that correspond to a monolayer. The derivative is easily evaluated from Eq. (4)

$$J = \alpha\sqrt{\frac{2}{\gamma + 1}}\sqrt{\frac{D}{\tau}} \tag{8}$$

In the case of multiple pores, the required flow rate per pore will be less than that given by Eq. (8). A system of pores will produce a coverage more uniform than that of Eq. (4), yielding a smaller value for $d\theta/dx$. However, the total flow from all the pores must increase as their density increases, because for smaller values of d, the inter-pore spacing, higher values for θ will result. Thus, the evaporation rate, given by θ^γ/τ, will be greater, and a greater net replenishment rate will be required.

Equations (4), (6), and (8) indicate the importance of the parameters D, τ, and d to the operation of a dispenser cathode.

B. TRANSPORT INSIDE THE PORES

With the passage of time, the barium in the porous matrix will gradually be depleted by evaporation, requiring the barium to be transported from ever greater depths before it reaches the pore opening. Rittner [3] has presented a model of internal transport based entirely on vapor transport by Knudsen flow. It is our intention to demonstrate that surface diffusion along the internal walls of the pores is probably the dominant transport mechanism. The issue is significant, since Knudsen flow is proportional to the pore radius r, whereas diffusive flow is inversely proportional to r. Thus, these mechanisms would have a different impact on the cathode design criteria concerning porosity.

Knudsen flow through the pores is described by

$$J_v = \frac{4r}{3}\sqrt{\frac{2}{\pi MkT}}\left|\frac{dP}{dz}\right| \tag{9}$$

where dP/dz is the pressure gradient in the direction of flow, z, and M, k, and T have their usual meanings. In comparison, surface diffusion, in terms of atoms per cross sectional area of the pore, is

$$J_D = -\alpha D \frac{d\theta}{dz}\frac{2\pi r}{\pi r^2} = \frac{2\alpha D}{r}\left|\frac{d\theta}{dz}\right| \tag{10}$$

In order to compare these two flow rates, we assume that the two types of flow occur independently of one another. This means, in particular, that there is no net exchange of barium between the vapor and the condensed phases along the pore (except at the source end). Conservation of mass requires both J_v and J_D to be independent of z. Therefore, both P and θ are linear with z,

$$J_D = \frac{2\alpha D}{r}\frac{\theta_s - \theta_o}{\ell} \tag{11}$$

and

$$J_v = \frac{4r}{3}\sqrt{\frac{2}{\pi MkT}}\frac{P_s - P_o}{\ell} \tag{12}$$

where ℓ is the distance from the active source of barium to the pore opening, s is the source end inside the pore, and o is the open end of the pore. We expect that $\theta_s - \theta_o > 1$ and $P_o > 0$. Thus,

$$J_D > \frac{2\alpha D}{r\ell} \tag{13}$$

$$J_v < \frac{4r}{3\ell}\sqrt{\frac{2}{\pi MkT}}P_s \tag{14}$$

In the case of Knudsen flow, the vapor atoms must eventually be intercepted and adsorbed on the current-emitting surface of the cathode before they can be of any use in lowering the work function. Thus, the effective flow is

$$J_v^e = \sigma(1 - R)\, J_v, \quad 0 < \sigma < 1, \quad 0 < R < 1 \tag{15}$$

where σ is the fraction of vapor atoms that strike the surface, and R is the fraction that is reflected without sticking.

We expect the pressure at the source end of the pore, P_s, to be less than the equilibrium vapor pressure, P_e, of the barium. Thus, at equilibrium, balancing the number of atoms that are leaving the condensed state ($\theta > 1$) with the number arriving yields the relation

$$\frac{\alpha}{\tau} = \frac{1 - R}{\sqrt{2\pi MkT}} P_e > \frac{1 - R}{\sqrt{2\pi MkT}} P_s \tag{16}$$

or

$$P_s < \frac{\sqrt{2\pi}\, MkT}{1 - R}\, \frac{\alpha}{\tau} \tag{17}$$

Equations (13), (14), (15), and (17), with $L = \sqrt{D\tau}$, yield

$$\frac{J_o}{J_v^e} > \frac{3\, D\tau}{4\sigma r^2} = \frac{1}{\sigma}\,\frac{3}{4}\left(\frac{L}{r}\right)^2 \tag{18}$$

The maintenance of an adequate layer of barium on dispenser cathodes would imply that, at the very least, $L > 2r$. Thus, we expect that

$$\frac{J_D}{J_v^e} > \frac{3}{\sigma}, \quad 0 < \sigma < 1 \tag{19}$$

Equation (19) indicates that surface diffusion is the dominant internal transport mode.

III. LABORATORY MEASUREMENTS OF DIFFUSION

A. METHOD OF INVESTIGATION

Our measurements were made to determine the rates of diffusion and evaporation of monolayers and submonolayers of barium on tungsten surfaces and to establish how these rates are affected by parameters such as the density of crystal grain boundaries and the concentration of impurity atoms. Although much work has been performed to evaluate the evaporation characteristics of barium on tungsten [7,1], less has been done to measure the diffusion coefficient. Furthermore, previous measurements of D still leave unanswered questions because of experimental constraints. Field emission microscopy studies [8,9], for example, have been confined to oxygen-free surfaces and do not yield a well-defined value for D near $\theta \approx 1$ because of geometric constraints. Furthermore, values for D measured at low coverages ($\theta << 1$) are of limited value in gaining an understanding of the behavior at higher coverages [10]. Techniques that are based on the measurement of work function ϕ [11, 12], however, do not measure θ directly but rely on empirical relationships between ϕ and θ which are dependent on impurity concentrations. Our technique, which makes use of a scanning Auger microprobe (SAM), permits the direct observation of barium diffusion on well-defined samples in the presence of oxygen and other elements.

The technique that we are using involves monitoring the smearing out of an initial step-function distribution of barium on a tungsten coupon. The initial distribution is prepared by masking one-half of a tungsten coupon while barium is deposited on the other half by vapor deposition. The barium is deposited to a thickness of approximately one monolayer (6.2×10^{14} atoms/cm^2) as monitored with a quartz crystal microbalance. With subsequent heat treatment, the smearing out of the initial coverage discontinuity provides a measure of D, while the decrease in the coverage in the plateau region (Figure 2) permits a determination of τ.

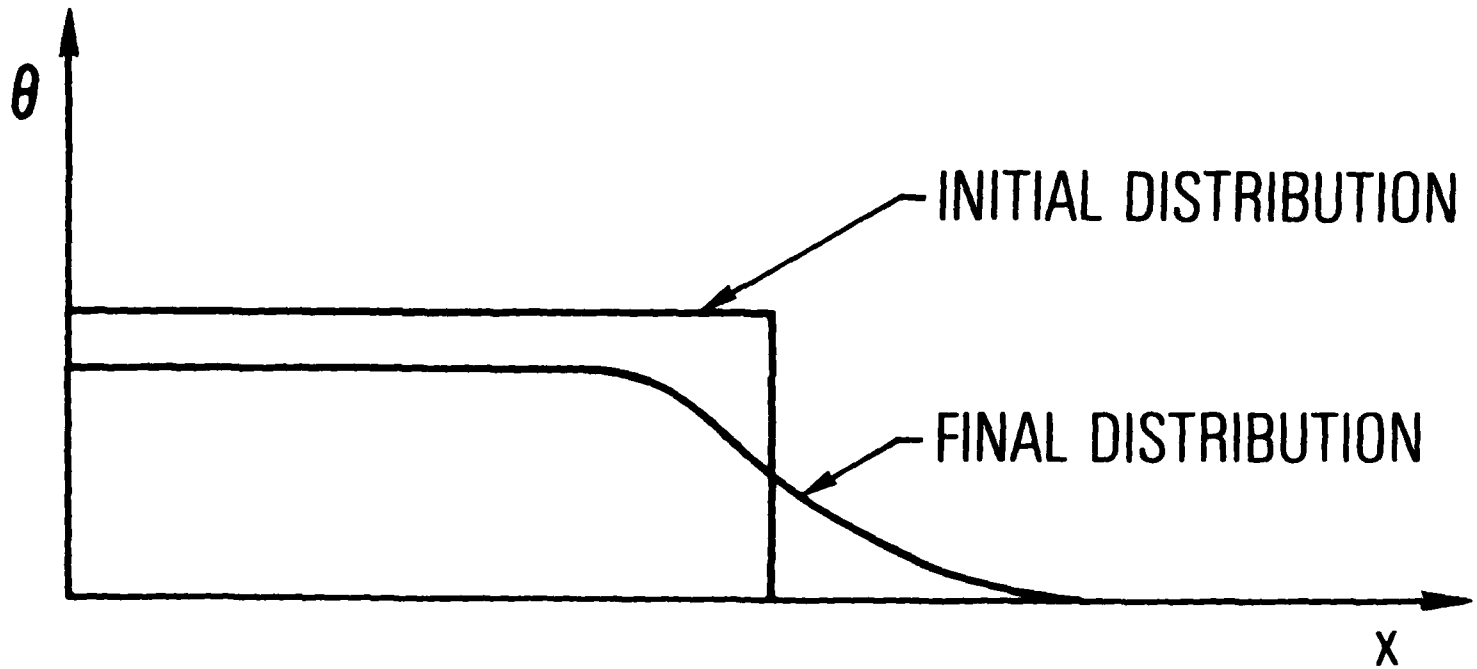

Fig. 2. Initial and Final Barium Distribution Profiles on a Tungsten Coupon

In particular, if the diffusion occurred without appreciable evaporation, an analysis of the final coverage profile (θ versus distance) can yield the dependence of the diffusion coefficient on θ with the use of the Boltzman-Matano equation [13]

$$D(\theta) = - \frac{1/2t \int_{\theta_0}^{\theta} x \, d\theta'}{(d\theta/dx)_{\theta'=\theta}} \tag{20}$$

with

$$\int_{\theta_0}^{\theta_1} x \, d\theta' = 0 \tag{21}$$

Since the SAM can detect low concentrations of elements on the tungsten surface, this technique also permits us to search for correlations between diffusion and evaporation rates and the presence of impurity elements. The impurity concentrations must be monitored while the diffusion is taking place, which necessitates the construction of a suitable hot stage for use in the SAM. Although we have constructed such a stage, our measurements, to date, have been of coupons with which the diffusion took place in a separate vacuum chamber prior to analysis.

The diffusion experiments were carried out on pure tungsten. The tungsten was either in the form of thin foils (6 mm on a side) or single crystal disks (6 mm in diameter). The tungsten was cleaned by the following procedure:

1. Immerse for 3 to 5 minutes in hot (150°C) trichloroethylene bath
2. Perform 3 to 5 minute ultrasonic cleaning in acetone and xylene
3. Rinse with acetone
4. Perform 3 to 5 minute ultrasonic cleaning in a solution of "Microwash"
5. Rinse with hot distilled water
6. Blow dry with N_2 gas
7. Heat samples to 1000°C for one hour in vacuum (10^{-4} N/m^2)

Subsequent to this cleaning, the barium was vapor deposited on one-half of the sample. The barium was deposited to a thickness of approximately one

monolayer (6.2×10^{14} atom/cm^2) as monitored with a quartz crystal microbalance. Both the vapor deposition and the subsequent diffusion were carried out in a bell jar pumped with an oil diffusion pump. The vacuum was on the order of 2.5×10^{-4} N/m^2.

The diffusion was carried out by placing the samples on a quartz substrate, which was mounted directly above a graphite heating element. In this geometry, the sample is not in an enclosure, i.e., the region above the samples is open. Thus, evaporated barium atoms should condense on room temperature surfaces in the bell jar and not be re-emitted back toward the sample. The graphite heater was designed to provide uniform heating over a square area 4.0 cm on a side. The temperature of the sample during the diffusion was determined by monitoring a chromel-alumel thermocouple that was spot welded to an identical sample. This latter sample was placed next to the diffusion sample.

Diffusion experiments have been performed at 900 and 950°C. These are 100 to 150°C lower than typical cathode operating temperature. Higher temperature measurements are planned with the use of the in-situ hot stage.

B. RESULTS

Our measurements were performed on polycrystalline tungsten foils (99.95% pure) and on polished, annealed tungsten single crystals. The (110) orientation was chosen for the latter, since that is the predominant orientation for polycrystalline tungsten. On the surface, in addition to the barium, oxygen, and tungsten, SAM measurements at room temperature reveal the presence of carbon, silicon, calcium, and nitrogen impurities, with only trace amounts (<2%) of calcium and nitrogen. Carbon is not expected to be present at diffusion temperatures but forms as an overlayer only upon cooling [6]. We hope to reduce silicon impurity levels by use of more exacting preparation techniques.

Maps of the barium distribution, as obtained from the SAM, in which brighter images correspond to greater barium concentrations, are reproduced in Figures 3 through 5. Figure 3 is a barium map of an unheated sample that displays the initial discontinuity. In addressing the effect of heating, we will discuss Figures 4 and 6 first, and then Figures 5 and 7. In Figures 4

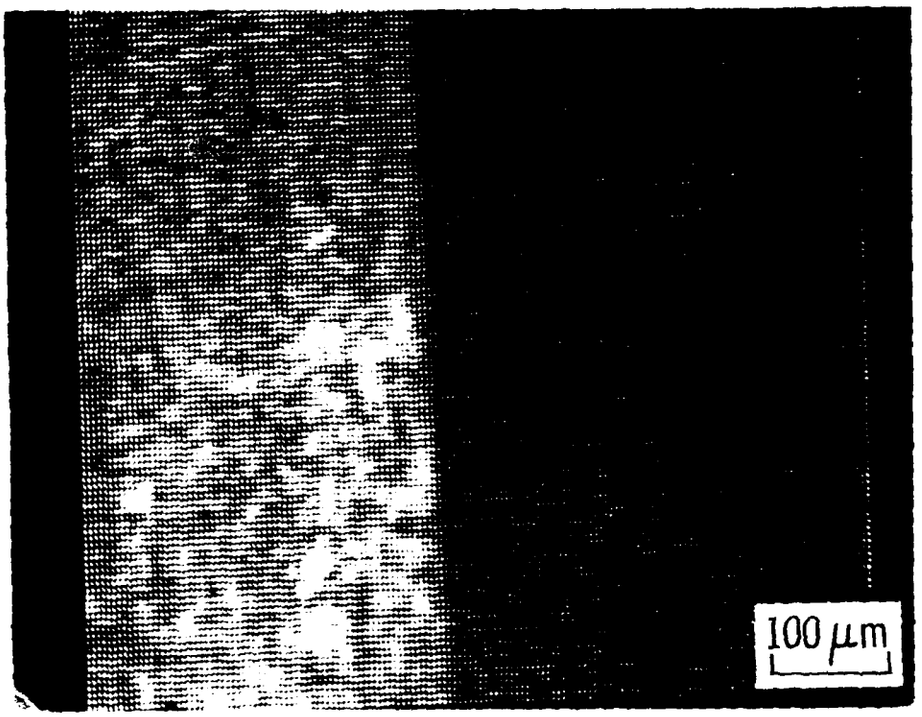

Fig. 3. SAM Map of an Unheated Coupon Indicating Initial Discontinuity in Barium Coverage

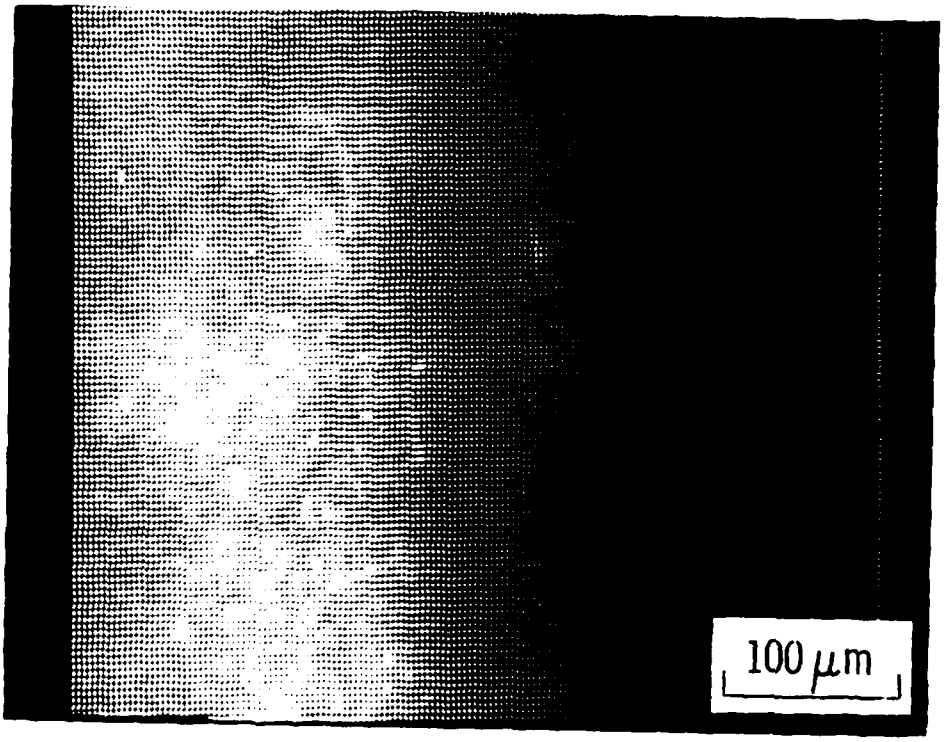

Fig. 4. SAM Barium Map of a Heated Coupon Exhibiting Gas-Like Diffusion

Fig. 5. SAM Barium Map of a Heated Coupon Exhibiting Liquid-Like Flow

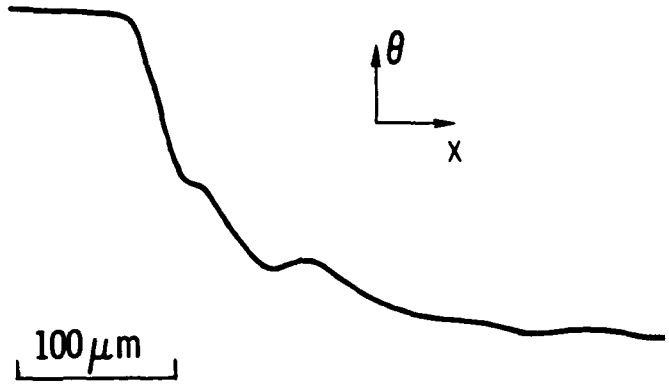

Fig. 6. Barium Distribution Profile for the System of Figure 4

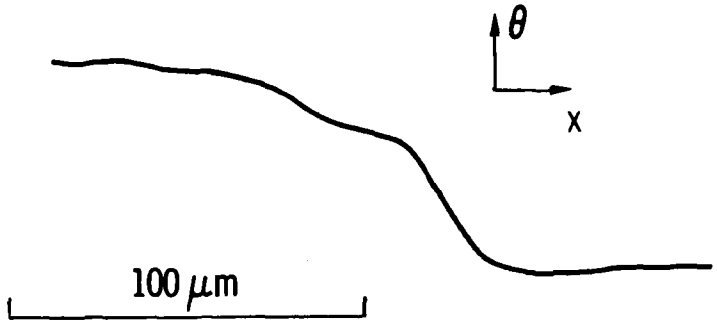

Fig. 7. Barium Distribution Profile for the System of Figure 5

and 6, we see a pattern typical of diffusive flow. The initial step-function distribution has smeared out uniformly in a manner describable by the diffusion equation

$$\frac{d\theta}{dt} = \frac{\partial}{\partial x}\left[D(\theta)\,\frac{\partial \theta}{\partial x}\right] \tag{22}$$

with a concentration-dependent diffusion coefficient. Since the evaporative loss was negligible for this particular case, Boltzman-Matano analysis of the profile of Figure 6 can be used to determine $D(\theta)$. This is displayed in the data points of Figure 8. In this figure, there is considerable scatter to the data for $\theta \leq 0.1$ because of the very weak Auger signal. The downturn in $D(\theta)$ for $\theta \leq 0.1$, therefore, may not actually exist.

Diffusive flow, as described by Eq. (22), indicates a system of atoms that are not mutually attractive to any significant degree. In fact, for $\theta > 0.1$, the dependence of $D(\theta)$ is closely described by Eq. (23) (solid line in Figure 8).

$$D = 6.75 \times 10^{-9}\,\frac{1-\theta}{\sqrt{\theta}}\ \mathrm{cm}^2/\mathrm{s} \tag{23}$$

The form of this equation was derived for the case of a two-dimensional gas at temperatures above its critical point [14]. Thus, we can think of this type of transport as that of a two-dimensional gas in which the individual atoms tend to move independently of each other (except when they get in each other's way).

In contrast, the type of movement exhibited in Figures 5 and 7 cannot be described by Eq. (22). The barium film has clearly moved about over the tungsten coupon, as is evident in Figure 5 from the irregular edge (which was initially straight as in Figure 3). However, the edge has not smeared out appreciably, i.e., there is still a relatively sharp step distribution. These observations imply that the barium atoms in this case are mutually attractive and are in a condensed phase. This transport of barium can be described as that of a very thin liquid film moving on a surface.

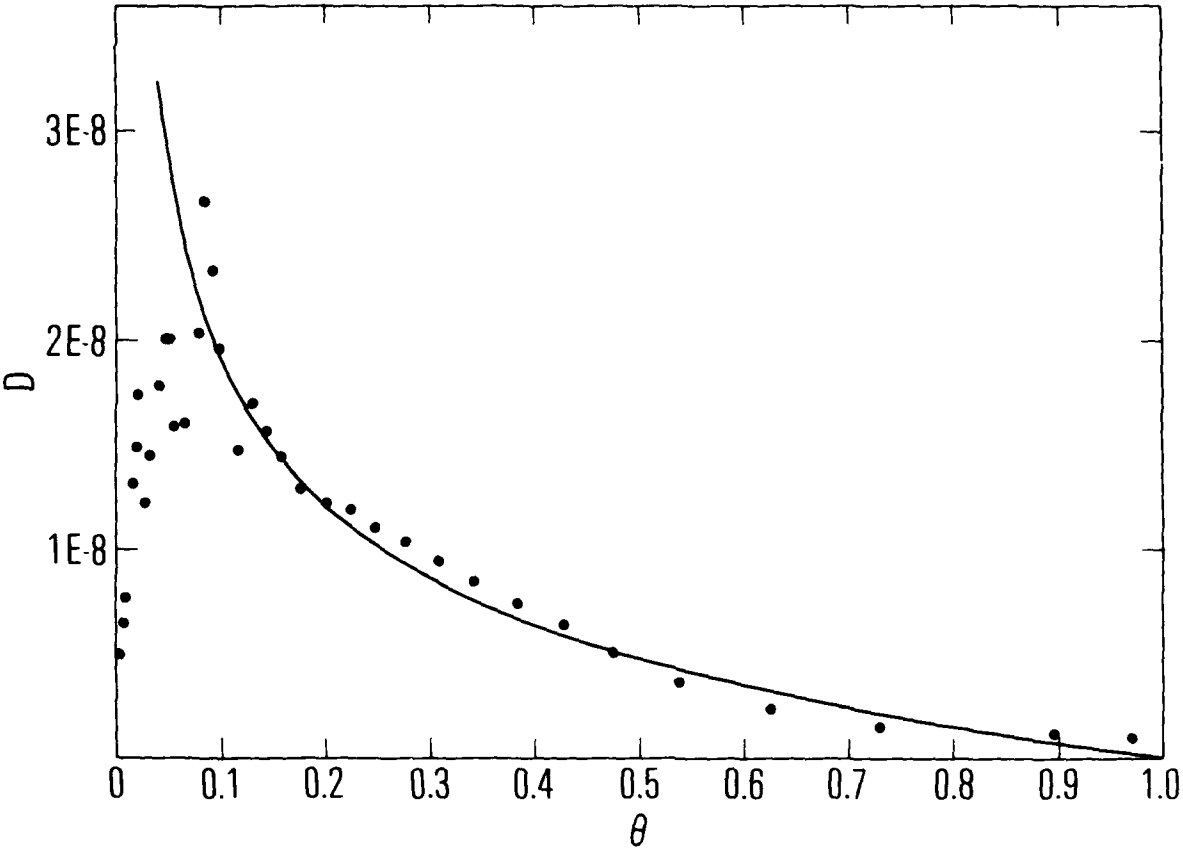

Fig. 8. D versus θ. Data points are obtained by performing a Boltzman-Matano analysis of the profile of Figure 4. Solid line is plot of Eq. (27)

Work is in progress to search for correlations between the observed types of barium transport and such surface parameters as impurity concentrations and grain boundary density. The former requires the use of a heatable SAM stage for concurrent measurements of diffusion and chemical compositions. Some studies on the latter, however, have been performed with negative results.

Two of the tungsten foils were annealed at 1500°C for three hours so larger crystals (~ 30 μm diam) could be grown, greatly reducing the grain boundary density on these coupons. A comparison of the diffusion and evaporation rates for these coupons with those of the normal foils (crystal size < 2 μm diam), with both types being heated simultaneously, indicated that there was no significant influence of grain boundary density on these processes. Also, both types of flow have been observed on both the polycrystalline foil and the single crystal coupons.

C. ANALYSIS

There are two types of barium transport on tungsten. A possible explanation for this behavior is that the surface transport is affected by the presence of some additional element. Oxygen is a likely candidate. Its relative abundance could control barium transport in the following way.

If the tungsten surface were not heavily oxidized (i.e., not WO_3), a reaction such as

$$BaO + W \rightarrow Ba + \cdots$$

or

$$BaO + WO_2 \rightarrow Ba + \cdots$$

could take place, as suggested previously [15]. This reaction should produce barium ions whose mutual repulsion would cause them to disperse in the same manner as a two-dimensional gas. The reaction would not occur if the tungsten were already in the form WO_3. The absence of the reaction would not of itself result in liquid-like flow. However, the phase diagram of the system $(BaO)_x (WO_3)_{1-x}$ reveals a low melting temperature (935°C) eutectic for $x = 1/4$ [16]. Thus, were the tungsten surface to be heavily oxidized, a liquid surface film of the above composition would form above 935°C. This would account for the liquid-like flow pattern we have observed.

REFERENCES

1. Forman, R., 1976, Surface Studies of Barium and Barium Oxide on Tungsten and its Application to Understanding the Mechanism of Operation of an Impregnated Tungsten Cathode, J. Appl. Phys. 47, p. 5272.

2. Haas, G. A., Gray, H. F., Thomas, R. E., 1975, Effects of S, Ba, and C on Impregnated Cathode Surfaces, J. Appl. Phys. 46, p. 3293.

3. Rittner, E. S., Rutledge, W. C., Ahlert, R. H., 1957, On the Mechanism of Operation of the Barium Aluminate Impregnated Cathode, J. Appl. Phys. 28, p. 1468.

4. Levi, R., 1953, New Dispenser Type Thermionic Cathode, J. Appl. Phys. 24, p. 233.

5. Moore, G. E., Allison, H. W., 1955, Adsorption of Strontium and of Barium on Tungsten, J. Chem. Phys. 23, p. 1609.

6. Springer, R. W., Haas, T. W., 1974, Auger Electron Spectroscopy Study of Cathode Surfaces During Activation and Poisoning. I. The Barium-on-Oxygen-on-Tungsten Dispenser Cathode, J. Appl. Phys. 45, p. 5260.

7. Muller, R., Wassmuth, H. W., 1973, Desorption Kinetics of Alkaline Earth Ad-Particles on Tungsten with Variation of the Oxygen Surface Coverage, Surf. Sci. 34, p. 249.

8. Becker, J. A., Hartman, C. D., 1953, Field Emission Microscope and Flash Filament Techniques for the Study of Structure and Adsorption on Metal Surfaces, J. Phys. Chem. 57, p. 153.

9. Benjamin, M., Jenkins, R. O., 1942, The Distribution of Autoelectronic Emission from Single Crystal Metal Points. II. The Adsorption, Migration and Evaporation of Thorium, Barium, and Sodium on Tungsten and Molybdenum, Proc. R. Soc. London A180, p. 225.

10. Graham, W. R., Ehrlich, G., 1974, Surface Diffusion of Atom Clusters, J. Phys. F4, p. L212.

11. Schaefer, D. S., White, J. E., 1952, Physical Processes in the L Cathode, J. Appl. Phys. 23, p. 669.

12. Vedula, Y. S., Garrilyuk, V. M., Margulis, N. D., 1959, Electronic and Adsorption Properties of a Film of Barium Atoms on a Tungsten Surface Covered by Oxygen, Fiz. Tver, Tela 1, p. 1717.

13. Butz, R., Wagner, H., 1977, Diffusion of Oxygen on Tungsten, Surf. Sci. 63, p. 448.

14. Coulomb, J. P., Bienfait, M., Thorel, P., 1977, Study of the Mobility of an Hypercritical Two-Dimensional Fluid by Quasi-Elastic Neutron Scattering, J. Phys. 31, p. C4-31.

15. Rutledge, W. C., Rittner, E. S., 1957, Studies on the Mechanism of Operation of the L Cathode, J. Appl. Phys. 28, p. 167.

16. Chang, L. L. Y, Scroger, M. G., and Phillips, B., 1966, Alkaline Earth Tungstate: Equilibrium Instability in the M-W-O Systems, J. Am. Ceram. Soc. 49, p. 385.

LABORATORY OPERATIONS

The Laboratory Operations of The Aerospace Corporation is conducting experimental and theoretical investigations necessary for the evaluation and application of scientific advances to new military space systems. Versatility and flexibility have been developed to a high degree by the laboratory personnel in dealing with the many problems encountered in the nation's rapidly developing space systems. Expertise in the latest scientific developments is vital to the accomplishment of tasks related to these problems. The laboratories that contribute to this research are:

Aerophysics Laboratory: Launch vehicle and reentry aerodynamics and heat transfer, propulsion chemistry and fluid mechanics, structural mechanics, flight dynamics; high-temperature thermomechanics, gas kinetics and radiation; research in environmental chemistry and contamination; cw and pulsed chemical laser development including chemical kinetics, spectroscopy, optical resonators and beam pointing, atmospheric propagation, laser effects and countermeasures.

Chemistry and Physics Laboratory: Atmospheric chemical reactions, atmospheric optics, light scattering, state-specific chemical reactions and radiation transport in rocket plumes, applied laser spectroscopy, laser chemistry, battery electrochemistry, space vacuum and radiation effects on materials, lubrication and surface phenomena, thermionic emission, photosensitive materials and detectors, atomic frequency standards, and bioenvironmental research and monitoring.

Electronics Research Laboratory: Microelectronics, GaAs low-noise and power devices, semiconductor lasers, electromagnetic and optical propagation phenomena, quantum electronics, laser communications, lidar, and electro-optics; communication sciences, applied electronics, semiconductor crystal and device physics, radiometric imaging; millimeter-wave and microwave technology.

Information Sciences Research Office: Program verification, program translation, performance-sensitive system design, distributed architectures for spaceborne computers, fault-tolerant computer systems, artificial intelligence, and microelectronics applications.

Materials Sciences Laboratory: Development of new materials: metal matrix composites, polymers, and new forms of carbon; component failure analysis and reliability; fracture mechanics and stress corrosion; evaluation of materials in space environment; materials performance in space transportation systems; analysis of systems vulnerability and survivability in enemy-induced environments.

Space Sciences Laboratory: Atmospheric and ionospheric physics, radiation from the atmosphere, density and composition of the upper atmosphere, aurorae and airglow; magnetospheric physics, cosmic rays, generation and propagation of plasma waves in the magnetosphere; solar physics, infrared astronomy; the effects of nuclear explosions, magnetic storms, and solar activity on the earth's atmosphere, ionosphere, and magnetosphere; the effects of optical, electromagnetic, and particulate radiations in space on space systems.